Electronic Supplementary Material (ESI) for Green Chemistry.

Supplementary Information

Cathode electrolysis for the comprehensive recycling of spent lithium-ion batteries

Jingjing Zhao[a], Jiakang Qu[a], Xin Qu[a], Shuaibo Gao[a], Dihua Wang[a,b,c], Huayi Yin [a,b,c*]

a. School of Resource and Environmental Science, Wuhan University, Wuhan, 430072, China.

b. Joint Center of Green Manufacturing of Energy Storage Materials of Wuhan University and Chilwee, Wuhan 430072, China.

c. International Cooperation Base for Sustainable Utilization of Resources and Energy in Hubei Province, Wuhan University, Wuhan 430072, China.

*Corresponding author. Email: wangdh@whu.edu.cn (Dihua Wang)

*Corresponding author. Email: yinhuayi@whu.edu.cn (Huayi Yin)

Number of pages: 21

Number of figures: 20

Number of tables:7

Supplementary Figures

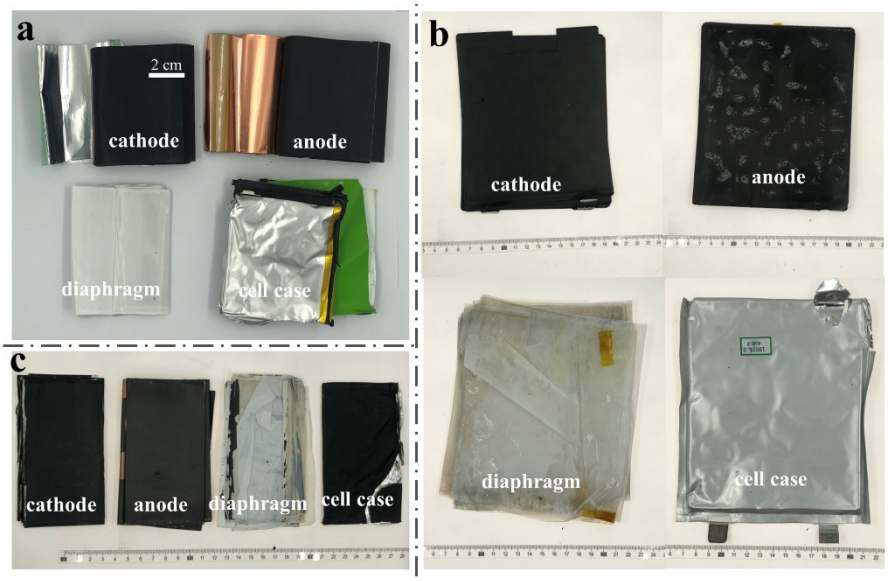

Fig. S1 Digital photographs of different parts of spent LIBs after disassembly. (a) LCO, (b) LMO, and (c) NCM.

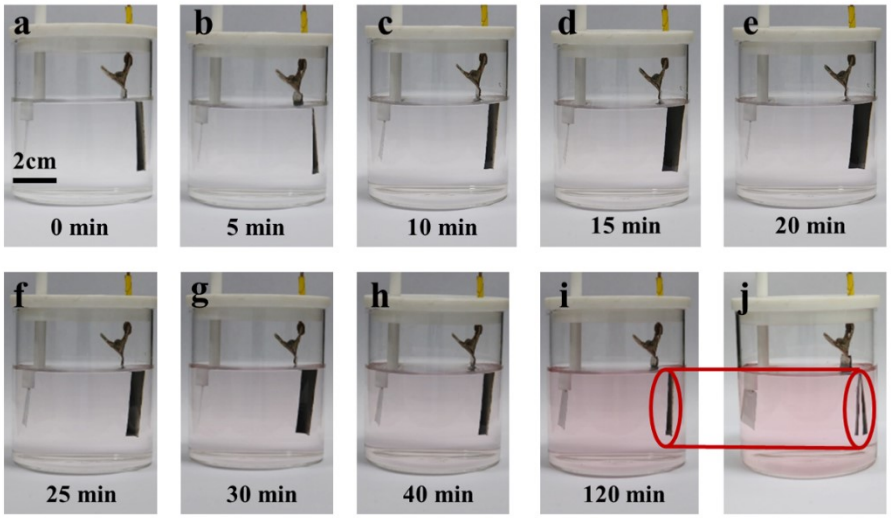

Fig. S2 Digital pictures of the solution soaked with LCO in 0.5 M H_2SO_4 at different times. (a) 0 min, (b) 5 min, (c) 10 min, (d) 15 min, (e) 20 min, (f) 25 min, (g) 30 min, (h) 40 min, (i) 120 min, and (j) separation.

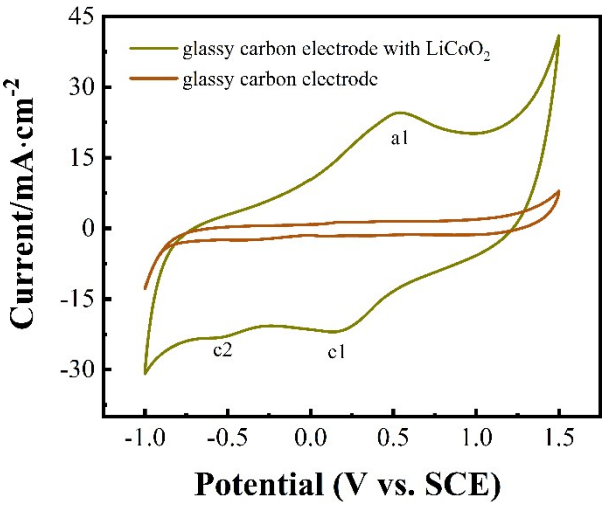

Fig. S3 Cyclic voltammograms of glassy carbon electrode decorated without/with $LiCoO_2$ powder in 0.5 M H_2SO_4 solution at room temperature, the scan rate is 100 mV s^{-1}.

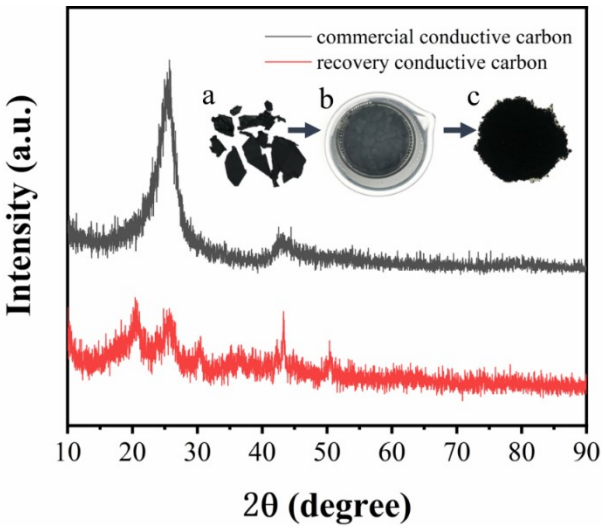

Fig. S4 XRD patterns of commercial conductive carbon and recovered conductive carbon. (a, b) the inset of picture of conductive carbon and PVDF after electrolysis, (c) the mixture of recycling conductive carbon and PVDF after grinding.

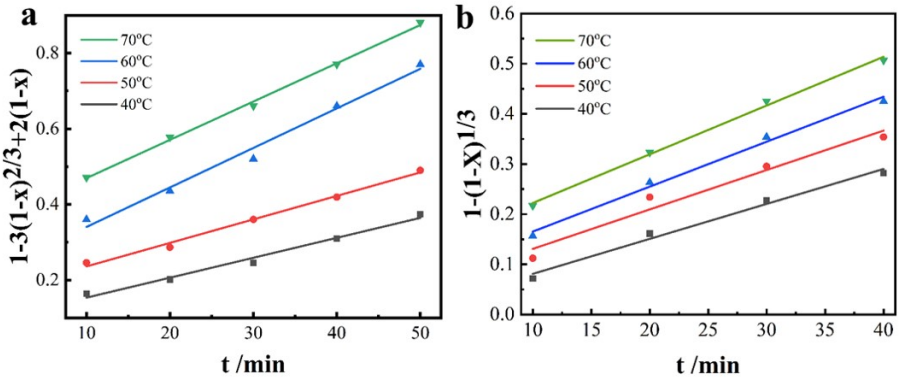

Fig. S5 Kinetic fitting of (a) Li and (b) Co of LCO at 2 V, in the 0.5 M H_2SO_4 solution at different temperatures.

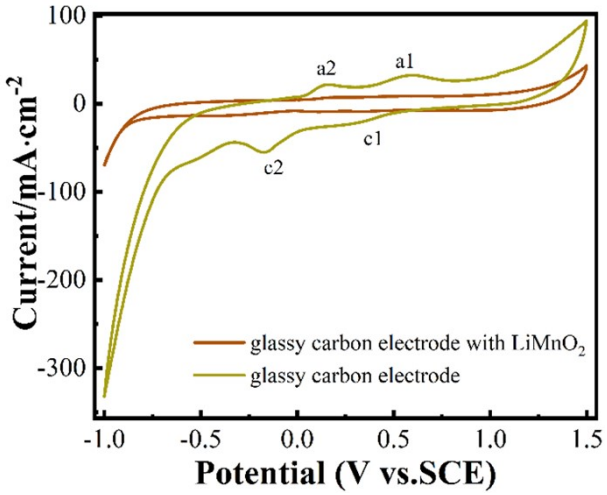

Fig. S6 Cyclic voltammograms of the glassy carbon electrode decorated without/with LMO powder in 0.5 M sulfuric solution.

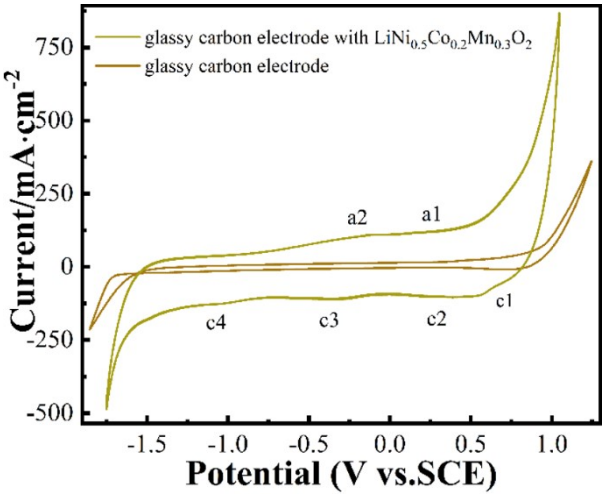

Fig. S7 Cyclic voltammograms of the glassy carbon electrode decorated without/with NCM powder in 0.5 M sulfuric solution.

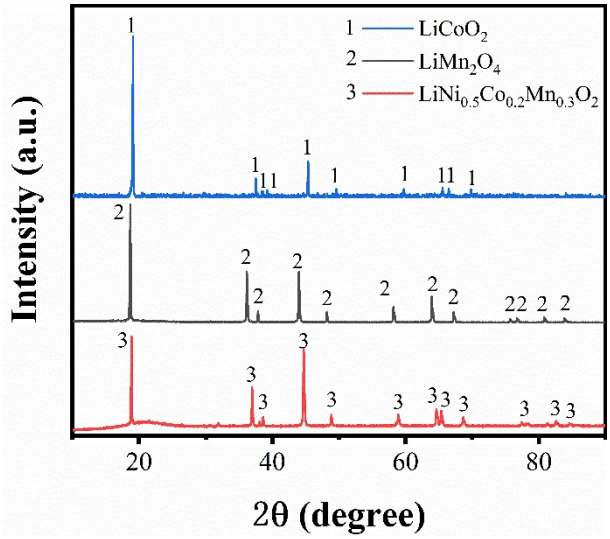

Fig. S8 XRD patterns of regenerative LCO, LMO, and NCM materials.

Preparation of re-LMO: During the high-temperature solid-state synthesis, the mole ratio of LiOH to manganese oxide ($Mn(OH)_2/MnO_2$) was 1.05 : 2. After ball-milling, the sample was preheated at 450 ℃ for 2 h under vacuum, and then calcinated at 800 ℃ for 24 h to prepare re-LMO (**Fig. S8**).

Preparation of re-NCM: The collected cathode materials ($Co(OH)_2$, $Ni(OH)_2$, and

$Mn(OH)_2/MnO_2$) were calcined at 800 ℃ for 1 h to prepare the precursor of Ni, Co, and Mn (atomic ratio of 5 :2 :3) under vacuum. The proportion of Li/transition metal was 1.05 : 1 (atomic ratio), the re-NCM523 was regenerated by a solid-state sintering at 950 ℃ for 16 h (**Fig. S8**).

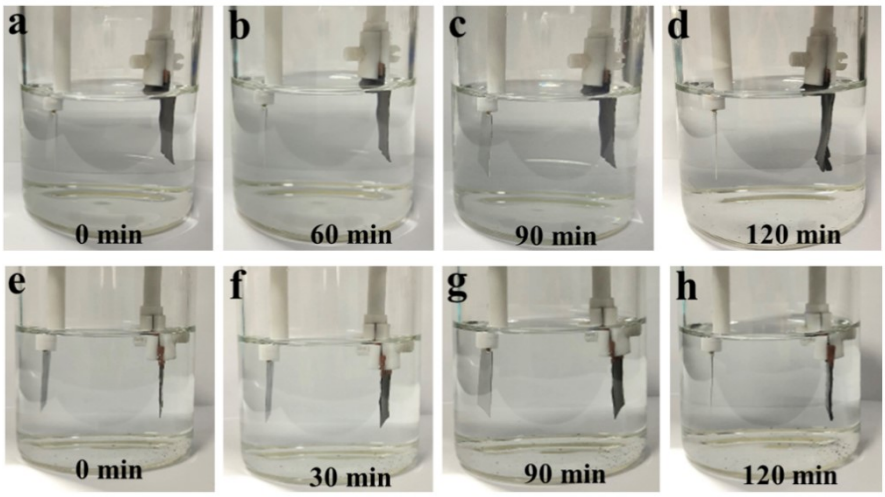

Fig. S9 Digital pictures of the solution soaked with LMO in 0.5 M H_2SO_4 for (a) 0 min, (b) 60 min, (c) 90 min and (d) 120 min. Digital pictures of the solution soaked with NCM in 0.5 M H_2SO_4 for (e) 0 min, (f) 60 min, (g) 90 min and (h) 120 min.

In a soaking experiment, no color change of the solution, and the cathode film started to separate from the Al substrate at 120 min.

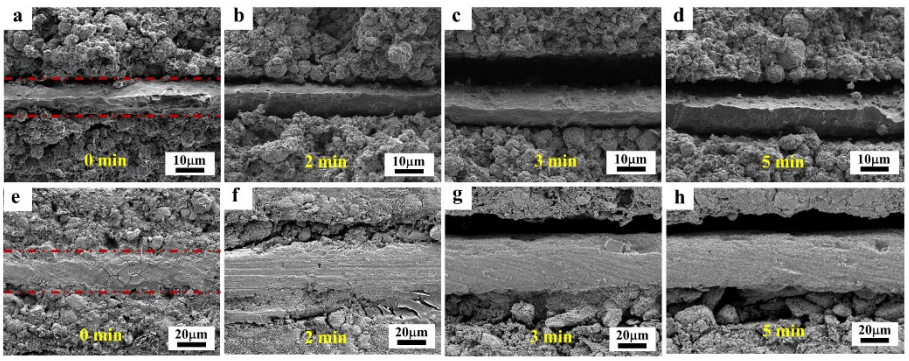

Fig. S10 SEM images of the LMO battery cathode cross-section of electrolysis for (a) 0 min, (b) 2 min, (c) 3 min, and (d) 5 min. SEM images of the NCM battery cathode cross-section of electrolysis

for (e) 0 min, (f) 2 min, (g) 3 min, and (h) 5 min.

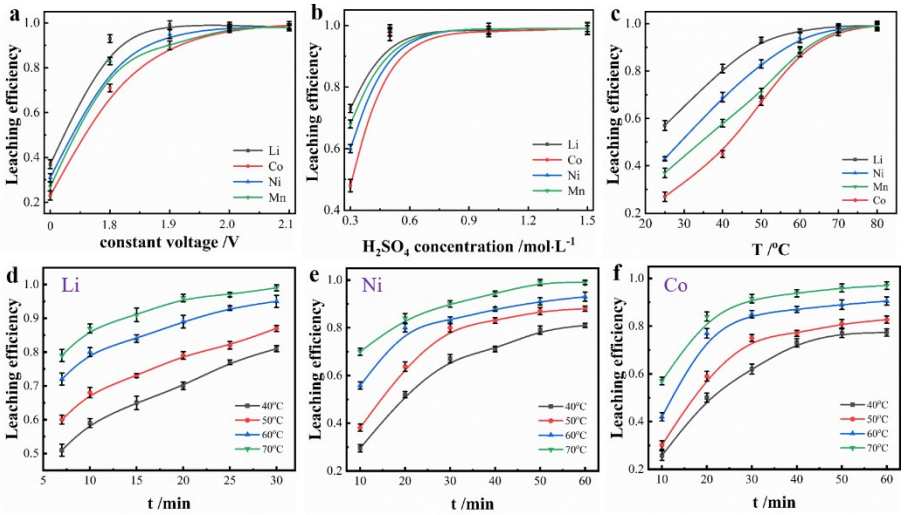

Fig. S11 Leaching kinetics. (a), Voltage (70 ℃, 0.5 M H_2SO_4, for 90 min). (b), H_2SO_4 concentration (70 ℃, 2 V, for 90 min). (c), temperature (2 V, 0.5 M H_2SO_4, for 90 min). effects of temperature on the leaching of Li (d), Ni (e) and Co (f) (70 ℃, 0.5 M H_2SO_4, 2 V).

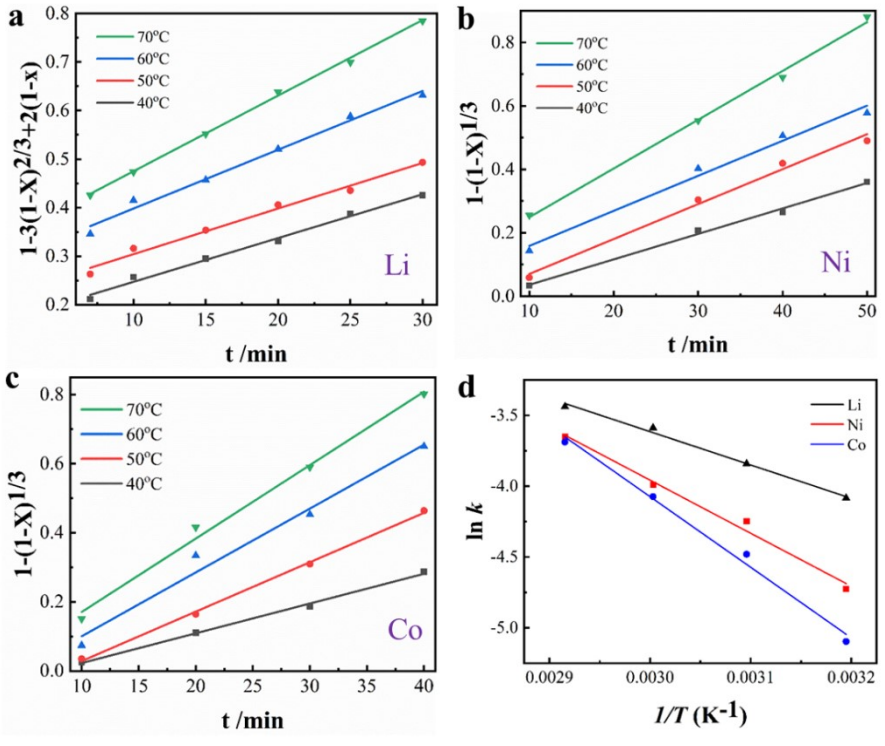

Fig. S12 Kinetics fitting. Kinetic fitting of (a) Li, (b) Ni, and (c) Co of NCM at 2V, in the 0.5 M

H_2SO_4 solution at different temperatures. (d) Arrhenius fitting lines of *ln k* as a function of *1/T* for Li, Ni and Co.

Compared with soaking, electrons drived the dissolution of LMO and NCM in H_2SO_4 solution. Since the weight of LMO and NCM accounted for 80 wt.% of the total cathode materials, the cathodic leaching led to the film separation.

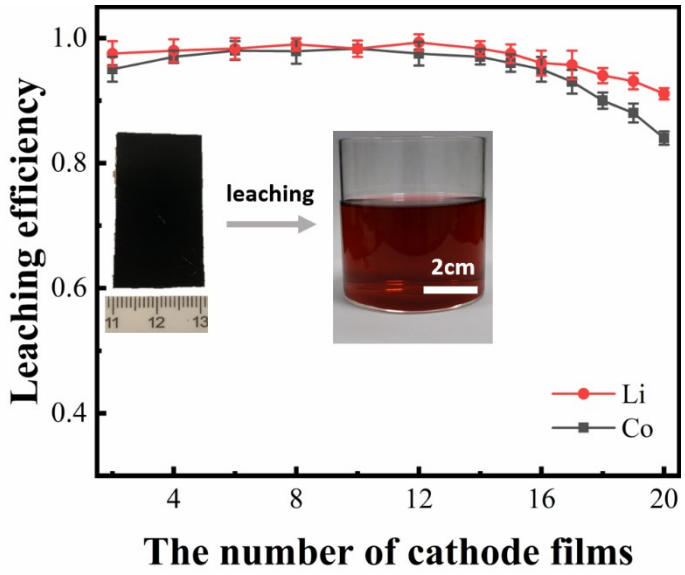

Fig. S13 The leaching efficiency as a function of the number of cathode films in the same solution.

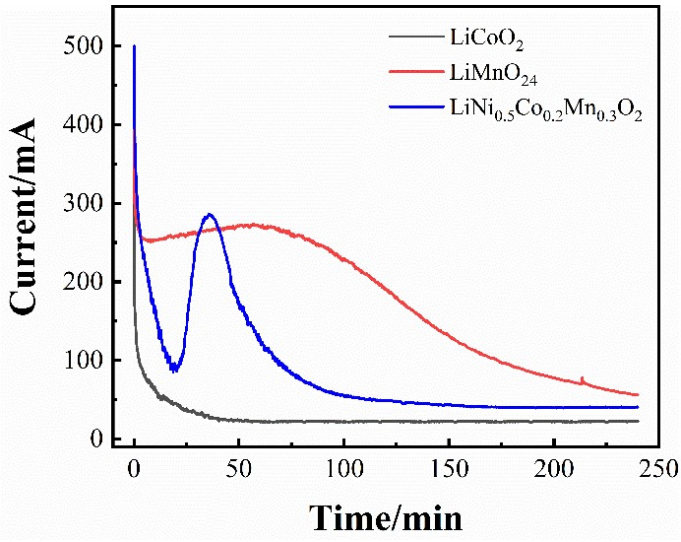

Fig. S14 Current curves of LCO, LMO, and NCM in scaled-up experimental conditions (2V, 70 ℃, 0.5 M H_2SO_4).

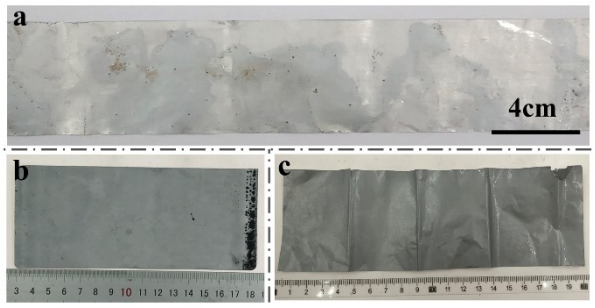

Fig. S15 Digital photographs of recycled Al foil at scaled-up experiments. Recycled from (a) LCO, (b) LMO, and (c) NCM.

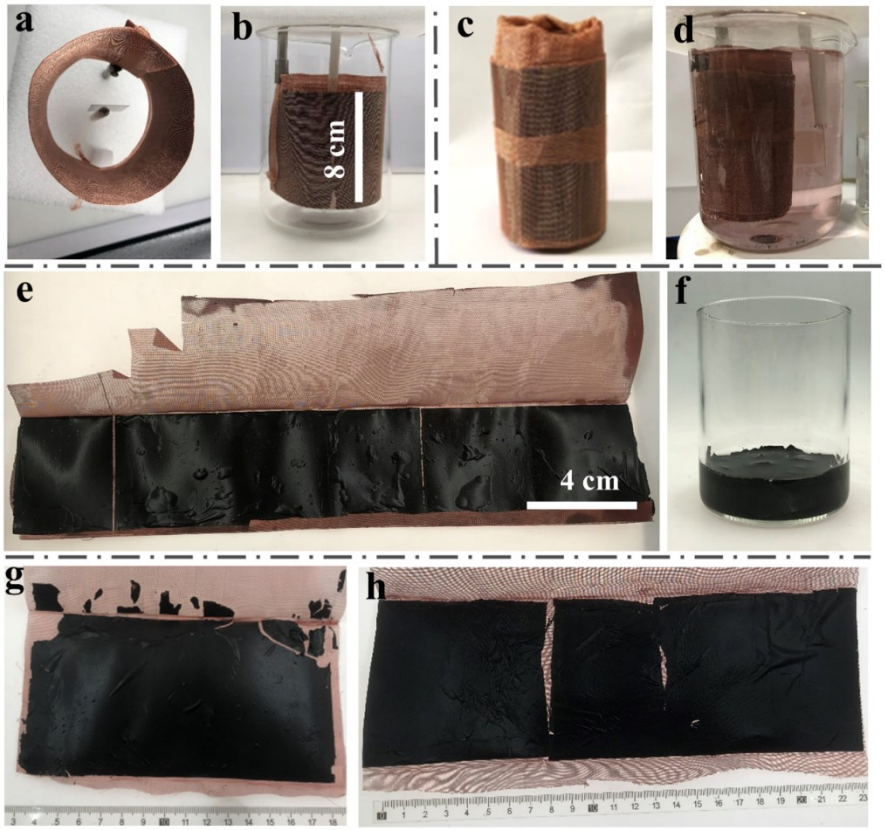

Fig. S16 Digital photographs of electrolysis. (a and b) Top view and side view of the electrolytic device, (c) the electrolytic cathode, (d) and electrolytic device. (e and f) Electrode materials of LCO after electrolysis at the scale-up experiment. Electrode materials of (g) LMO and (h) NCM after electrolysis at scaled-up experiments.

As shown in **Fig. S14**, the device (**Fig. S14b**) where the Pt electrode was in the center of the cathode was used to calculate the leaching efficiency of Li, Co, Mn, and Ni. The larger solid-liquid contact area was helpful to increase current efficiency and leaching efficiency. The device (**Fig. S14d**) where the Pt electrode was outside of the cathode was used to record videos of leaching processes of LCO, LMO, and NCM.

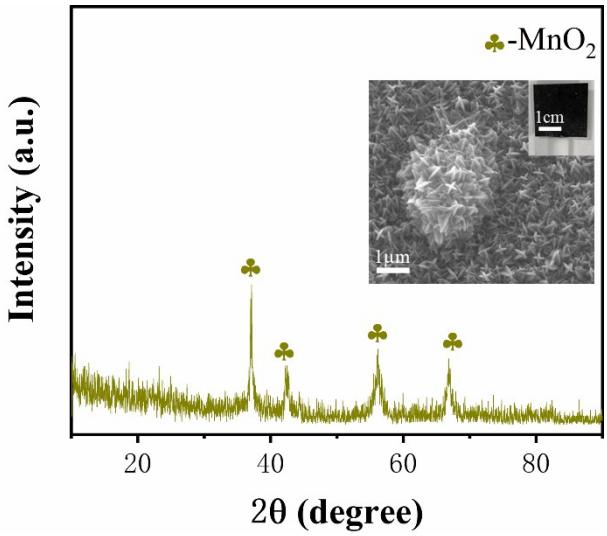

Fig. S17 XRD patterns and SEM image of MnO_2 precipitated on Pt electrode.

The calculate of the leaching efficiency, the current efficiency, and the utilization efficiency, of LCO, LMO, and NCM are as follows:

Under the cell voltage of 2.0 V, the weight of Co^{2+} leached in 0.5 M solution was 9.08 g. The consumed charge was 4217.4 mAh, and the sulfuric acid in the leachate was 0.25 mol. According to **Eq. 9** and **Eq. 10,** the current efficiency, and the utilization efficiency of sulfuric acid were calculated as follows (**Eqs. S1, S2**):

$$\tau = \frac{n_e F}{Q} \times 100\% = \frac{\frac{9.08\ g}{59\ g/mol} \times 96485\ C/mol}{3.6 \times 4217.4\ mAh} \times 100\% = 97.8\% \quad \text{(S1)}$$

$$\sigma = \frac{c_1 * V_1 \times \frac{3}{2}}{c_2 * V_2} \times 100\% = \frac{\frac{9.08\ g}{59\ g/mol} \times \frac{3}{2}}{0.25\ mol} \times 100\% = 92.3\% \quad \text{(S2)}$$

where τ is the current efficiency, n_e is the consumed amount of $LiCoO_2$ (mol), F is Faraday constant, Q is the amount of the electricity recorded on the battery testing system, σ is the utilization of sulfuric acid, c_1 is the concentration of H^+ in the leachate, V_1 is the volume of leachate, c_2 is the concentration of sulfuric acid, and V_2 is the volume of sulfuric acid.

When the cathodic area of LMO film increased to 8 cm × 15 cm, the leaching efficiency of Li and Mn were 99.3% and 98% (the leaching efficiency of Mn was the sum of leaching Mn^{2+} in solution and MnO_2 precipitation at the anode), respectively. And the current efficiency of the cathodic reaction was 97.1%, the utilization of H_2SO_4 was 89.3% at 70 ℃, 2 V, and in 0.5 M H_2SO_4. As for NCM, the cathodic area of NCM was 8 cm × 20 cm, the leaching efficiency of Li^+, Ni^{2+}, Co^{2+}, and Mn^{2+} were 99.5%, 98.3%, 95.1%, and 97.3%, respectively. and the current efficiency of the cathodic reaction was 98.1%, the utilization of H_2SO_4 was 91.3% at 70 ℃, 2 V, and in 0.5 M

H_2SO_4.

Economic and environmental analysis

The EverBatt model, a closed-loop battery recycling model developed at Argonne National Laboratory[1], was used to conduct a techno-economic and life-cycle analysis of pyrometallurgical, hydrometallurgical, and biomass reduction recycling processes. Our analysis was focused on the total energy use and GHG emissions of the three recycling methods and did not include the emissions or energy associated with their use in electric vehicles. Moreover, the cost and revenue of the three recycling methods were modeled as well[2].

In the pyrometallurgical recovery process (**Fig. S16**), the spent lithium is sent to the smelter, the electrolyte and plastic in the battery are burned to provide heat; the graphite/carbon and aluminum in the battery are used as metal reducing agents and are oxidized; The cobalt, nickel, copper, and iron in the battery eventually go into matt; the remaining materials, including alumina, go into the slag. Co/Cu/Fe matte is further processed, and then the cobalt and nickel compounds are produced through solvent extraction and precipitation, which can be used in the production of cobalt and nickel cathode materials.

In the hydrometallurgical recovery process (**Fig. S17**), the discharged and separated waste batteries are crushed, and then subjected to a low-temperature calcination process to burn the binder and electrolyte; several physical separation processes separate aluminum, copper, and steel as metal fragments and Plastics; and the leaching process, followed by solvent extraction, and sometimes precipitation to produce Co compounds and potential lithium carbonate for the production of new

cathode materials.

In this study, EverBatt's general electro recovery process was modified to describe the electrolyte reduction recovery process, as shown in **Fig. S18**. In the recycling process, Li, Co, conductive carbon, and PVDF can be recovered from waste LIBs through disassembly, electrolyte reduction leaching. Please note that the entire process does not use high concentration acid and amount of alkali solutions, and works at moderate temperatures separates the electrode material from the current collector while keeping the current collector intact.

It is worth noting that the commercial pyrometallurgical flow chart and commercial hydrometallurgical flow chart here are obtained from Everbatt 2020 and are copied here for readers to understand[1, 3].

Evaluation of energy consumption and greenhouse gas emissions (GHGs)

Material input. The material requirements for these three recycling technologies are summarized in **Tab. S6**. The material requirements for general coke metallurgy and hydrometallurgical processes are obtained from EverBatt and copied here for readers' understanding. The material requirements for the electrolytic reduction recycling process are obtained according to our laboratory process.

Energy input. To calculate the life cycle environmental impact of the consumed (es) energy in the process, the life cycle analysis considers the environmental impact related to upstream fuel production and power generation, as well as the environmental impact related to on-site fuel combustion (such as diesel/natural gas combustion).

Process emissions. In the life cycle analysis, we also consider the environmental impacts associated with process emissions that are not related to fuel combustion. For these three recycling processes, the emissions from the process include those from material combustion and thermal decomposition.

Evaluation of potential revenue

The revenue calculation was based on the sales of recycled materials. The prices are obtained from EverBatt and listed in **Tab. S7**.

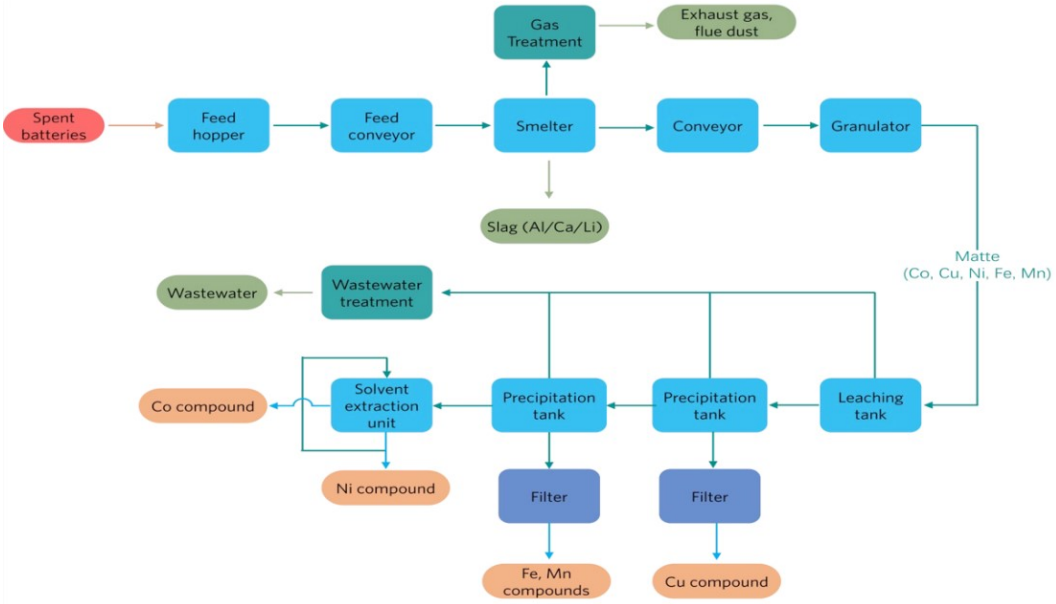

Fig. S18 Process diagram of a generic pyrometallurgical process.

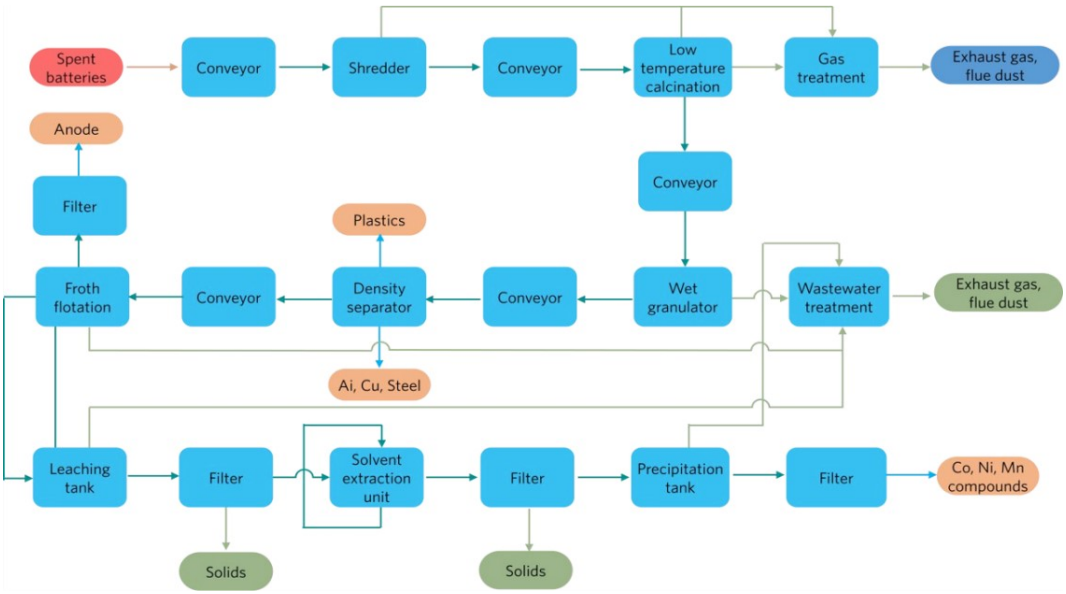

Fig. S19 Process diagram of a generic hydrometallurgical process.

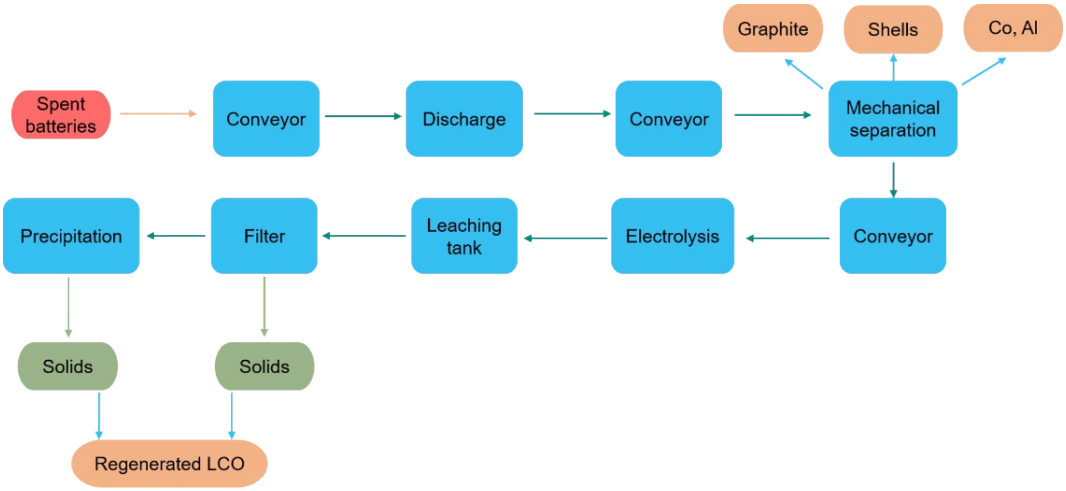

Fig. S20 Process diagram of a hydrometallurgical recovery process assisted by electrochemistry.

Supplementary Tables

Table S1 Summarization of typical sulfuric acid leaching processes.

Type of LIBS	Leaching agent	Temperature (℃)	S/L ratio ($g\ L^{-1}$)	Time (h)	Leaching efficiency (%)	utilization efficiency of acid (%)	utilization efficiency of agent (%)	Ref.
$LiCoO_2$	2 M H_2SO_4 + 2.0 vol % H_2O_2	60	33	2	Co:96.3	25.3	85.2	[4]
$LiCoO_2$	2 M H_2SO_4 + 5.0 vol % H_2O_2	80	50	1	Co>99	38.3	51.7	[5]
$LiCoO_2$	2 M H_2SO_4 + 5.0 vol % H_2O_2	75	100	1	Co:70	76.5	>99	[6]
$LiCoO_2$	2 M H_2SO_4 + 8.0 vol % H_2O_2	75	50	1	Co:98	15.3	32.3	[7]
$LiCoO_2$	4 M H_2SO_4 + 10.0 vol % H_2O_2	85	100	2	Co:95	38.3	51.7	[8]
$LiCoO_2$	3 M H_2SO_4	70	200	6	Co:98	51.0	-	[9]
$LiCoO_2$	4 M H_2SO_4	80	10	1	Co:99	10.2	-	[10]
$Li_4Ti_5O_{12}$	4 M H_2SO_4 + 20.0 vol % H_2O_2	80	25	4	Ti:98	9.5	13.9	[11]
$LiCoO_2$	electrochemical	70	-	1.5	Ni, Co, Mn>97	92.3	>99	-

Table S2 Kinetic parameters of Li and Co obtained from spent LIBs of different kinetic models at 2 V, in 0.5 M H_2SO_4 at different temperatures.

Temperature (°C)	Residue layer diffusion		Surface chemical reaction	
	Li		Co	
	k (min^{-1})	R^2	k (min^{-1})	R^2
40	0.00426	0.99347	0.00213	0.87512
50	0.00621	0.98775	0.00294	0.96748
60	0.00846	0.98731	0.00489	0.91425
70	0.01012	0.98659	0.00691	0.9238

Table S3 The activation energy (E_a) values of Li and Co obtained from spent LIBs.

Element	Slope	E_a (KJ/mol)	R^2
Li	-3137.9	26.089	0.98468
Co	-4349.1	36.158	0.98355

Table S4 Kinetic parameters of Li, Ni, and Co of Li and Co obtained from spent LIBs of different kinetic models at 2 V, in 0.5 M H_2SO_4 at different temperatures.

Temperature (°C)	Residue layer diffusion		Surface chemical reaction			
	Li		Ni		Co	
	k (min^{-1})	R^2	k (min^{-1})	R^2	k (min^{-1})	R^2
40	0.00738	0.99201	0.00886	0.97726	0.01083	0.99317
50	0.00941	0.98679	0.01431	0.99465	0.02006	0.98998
60	0.01211	0.98803	0.01849	0.94421	0.03011	0.98569
70	0.01406	0.99854	0.02597	0.99553	0.04427	0.99636

Table S5 The activation energy (E_a) values of Li, Ni and Co obtained from spent LIBs.

Element	Slope	E_a (KJ/mol)	R^2
Li	3008.17	25.01	0.98764
Ni	3773.1	31.37	0.97113
Co	4357.7	36.23	0.97485

Table S6 Materials requirements (kg) to recycle 1 kg of spent batteries through different recycling technologies.

Pyrometallurgy	Hydrometallurgy	Electro recycling
Hydrochloric acid	Ammonium hydroxide	Sulfuric acid
Hydrogen peroxide	Hydrochloric acid	Sodium hydroxide
Limestone	Hydrogen peroxide	Soda ash
Sand	Sodium hydroxide	
	Sulfuric acid	
	Soda ash	

Table S7 Value of recycled materials ($/kg).

	Pyrometallurgy	Hydrometallurgy	Electro recycling
Copper	0.92	0.92	0.92
Aluminum		0.12	0.12
Graphite		0.03	0.03
Co^{2+} in product	12.38	12.38	19.57

Supplementary Videos

Video S1 Scaled-up electrolysis LCO at 2V, 70 ℃ in 0.5 M H_2SO_4.

Video S2 Scaled-up electrolysis LMO at 2V, 70 ℃ in 0.5 M H_2SO_4.

Video S3 Scaled-up electrolysis NCM at 2V, 70 ℃ in 0.5 M H_2SO_4.

Reference:

1. Q. Dai, J. Spangenberger, S. Ahmed, L. Gaines, J. Kelly and M. Wang, *Argonne National Laboratory*, 2019.
2. P. Xu, Q. Dai, H. Gao, H. Liu, M. Zhang, M. Li, Y. Chen, K. An, Y. S. Meng, P. Liu, Y. Li, J. S. Spangenberger, L. Gaines, J. Lu and Z. Chen, *Joule*, 2020, **4**, 2609-2626.
3. P. Xu, Z. Yang, X. Yu, J. Holoubek, H. Gao, M. Li, G. Cai, I. Bloom, H. Liu, Y. Chen, K. An, K. Z. Pupek, P. Liu and Z. Chen, *ACS Sustain. Chem. Eng.*, 2021, **9**, 4543-4553.
4. X. Chen, C. Guo, H. Ma, J. Li, T. Zhou, L. Cao and D. Kang, *Waste Manage.*, 2018, **75**, 459-468.
5. L. Sun and K. Qiu, *J. Hazard. Mater.*, 2011, **194**, 378-384.
6. M. K. Jha, A. Kumari, A. K. Jha, V. Kumar, J. Hait and B. D. Pandey, *Waste Manage.*, 2013, **33**, 1890-1897.
7. D. A. Bertuol, C. M. Machado, M. L. Silva, C. O. Calgaro, G. L. Dotto and E. H. Tanabe, *Waste Manage.*, 2016, **51**, 245-251.
8. L. Chen, X. Tang, Y. Zhang, L. Li, Z. Zeng and Y. Zhang, *Hydrometallurgy*, 2011, **108**, 80-86.
9. Z. Takacova, T. Havlik, F. Kukurugya and D. Orac, *Hydrometallurgy*, 2016, **163**, 9-17.
10. Y. Yao, M. Zhu, Z. Zhao, B. Tong, Y. Fan and Z. Hua, *ACS Sustain. Chem. Eng.*, 2018, **6**, 13611-13627.
11. W. Tang, X. Chen, T. Zhou, H. Duan, Y. Chen and J. Wang, *Hydrometallurgy*, 2014, **147-148**, 210-216.